Cambridge iGEM22 Mathematical analysis and Modelling

October 9, 2022

1 Preamble - a mathematician's perspective

Our project epitomizes a wonderful marriage between theoretical and experimental approaches to engineering biological circuits. But an ambitious goal means no easy tasks! To build such a complicated feedback controller into E.coli chassis and demonstrate robust perfect adaptation (RPA), we understand the absolute importance of dissecting the system using theoretical/computational frameworks. This helped inform us of any envisioned caveats, cautions, and optimization rationales learned from in silico simulations and then guide our wet-lab implementation strategies.

Here, we show how the use of mathematical toolkit has enabled us to conduct several analyses of the system's properties, including dynamical stability, overshoot, and offset; and investigate the parameter space. This approach fosters a freshly different view to that of control theory. Yet, we shall demonstrate how both narratives perfectly complemented each other and impactfully serviced the real implementation as a whole.

In the discussion below, we will investigate RPA in both the activation and repression modules of the antithetic circuits to different extents. We relied mostly on simplified sets of ODEs to represent the system, as these are the most algebraically approachable.

2 RPA in activation module

2.1 Model and assumptions

We first consider the case for the activation module, of which the dynamical stability has been rigorously studied in the literature. The system of differential

equations is:

$$\begin{cases} \dot{x} & = \theta_1 z_1 - \gamma_p x \\ \dot{z}_1 & = \mu_1 - \eta z_1 z_2 \\ \dot{z}_2 & = \theta_2 x - \eta z_1 z_2 \end{cases} \tag{1}$$

Where θ_1 is the activation rate of controller z_1 acting on x, γ_p is the dilution rate of x, μ_1 is the constitutive production rate of z_1, η is the sequestration rate, and θ_2 is the activation rate of x acting on z_2. Both z_1 and z_2 are controller species responsible for maintaining the steady state of x. This is achieved through molecular titration, in which the two sequester/annihilate each other in a one-to-one ratio, rendering both inactive.
Here, a few core assumptions are made:

- The intrinsic removal rates of the process species z_1 and z_2 are omitted, or considered as negligible. In the case of bacterial chassis, active protein degradation is often slow, and this rate is mostly dominated by cytoplasmic dilution (so-called dilution rate) due to fast generation time. If the circuit was to be studied in S. *cerevisiae* or mammalian cells, then the dilution rate would not be as comparable as proteolysis. Regardless, this simplification would help simplify the steady-state of all species into clean analytic expressions.

- The production of x and z_2 are linearly proportional to z_1 and x through the single parameter θ_1 and θ_2, respectively. This would only be true if the concentrations of z_1 and x were significantly below saturation level, or within the regime of first-order kinetics. While the assumption is not particularly useful for implementation, its advantage is that the dynamics can be analyzed in a much simpler, but still informative, fashion.

- The parameters θ_1, θ_2 and μ_1 are generic aggregate variables that embed quantitative information about relevant biochemical processes such as transcription and translation. For example, the production rate of z_1 - μ_1, is governed collectively by multiple factors, including promoter strength, RBS strength, ribosome number and plasmid copy number. While this makes the precise calculation of these parameters challenging, we could make rough estimates of their range of orders of magnitude to screen the parameter space.

- The sequestration of z_1 and z_2 is irreversible and conforms to second-rate law of kinetics:

  $$z_1 + z_2 \xrightarrow{\eta} z_1 z_2$$

  where η acts as the rate constant. In other words, the dissociation rate of $z_1 z_2$ back to its constituent titrator species (reverse direction) is assumed negligible. This is justifiable for certain pairs of titrators of which the association constant K_a is above two orders of magnitude high. This is the case for our implementation using sigma-antisigma pairs (ECF20 - AS20 and ECF16 - AS16).

- The inducer concentration, used as a tuneable point, is embedded into the aggregate parameter θ_2 and remains constant over time, thus θ_2 is also unchanged. Typically, inducers would be used up by the cells or degraded internally and over time this reduces activation efficiency of promoter, but this would make the analysis more cumbersome as the parameter varies with time.

- Leaky expression of x and z_2 is negligible and its contribution is omitted from the equations. In fact, we were careful in selecting promoters with minimal leakiness for actual implementation.

From (1), we yield the equilibrium point at:

$$x_{eq} = \frac{\mu_1}{\theta_2},\ z_{1eq} = \frac{\mu\gamma_p}{\theta_1\theta_2},\ z_{2eq} = \frac{\theta_1\theta_2}{\eta\gamma_p} \tag{2}$$

Most importantly, by subtracting the third to the second equation in (1), we obtain that:

$$\dot{z}_1 - \dot{z}_2 = \mu_1 - \theta_2 x \Rightarrow \boxed{(z_1 - z_2)(t) = \theta_2 \int_0^t \frac{\mu_1}{\theta_2} - x(t')\,dt} \tag{3}$$

Relation (3) illustrates the perfect adaptation property implemented by this feedback controller. Intuitively, this occurs when the rate of z_1 precisely counterbalances that of z_2, or $\dot{z}_1 - \dot{z}_2 = 0$; and consequently, when $x_{eq} = \frac{\mu_1}{\theta_2}$ (for the RHS integral to vanish). Hence, we interpret that, under feedback adaptation, the steady state expression for x must be invariant and only dictated by two parameters μ_1 and θ_2, which are preset by the production strength and regulatory activation, respectively. Any deviation from this value would indicate that the system is no longer perfectly robust and is taking in the effect of perturbation.

2.2 Stability analysis

We are interested in understanding how the dynamic stability of the system changes within the parameter space and pinpoint the boundary that separates stability and instability. We shall show, for our particular implementation, that the system is intrinsically stable for both activation and repression modules. We adapted the analysis from Briat and Olsman, who has been of tremendous help to our modelling progress. Details on their support are documented on the Human Practice page. To start, we linearize the system by taking the Jacobian (J):

$$\dot{\vec{x}} = J\vec{x}$$

$$\therefore\ J = \begin{pmatrix} -\gamma & \theta_1 & 0 \\ 0 & -z_2\eta & -z_1\eta \\ \theta_2 & -z_2\eta & -z_1\eta \end{pmatrix}$$

where $\dot{\vec{x}} = (\dot{x}\ \dot{z_1}\ \dot{z_2})^T$ and $\vec{x} = (x\ z_1\ z_2)^T$. Further explanation on the mathematics of linearization is documented in control theory section.
Plugging in the equilibrium values, we obtain:

$$J = \begin{pmatrix} -\gamma & \theta_1 & 0 \\ 0 & -\frac{\theta_1\theta_2}{\gamma} & -\frac{\eta\mu\gamma}{\theta_1\theta_2} \\ \theta_2 & -\frac{\theta_1\theta_2}{\gamma} & -\frac{\eta\mu\gamma}{\theta_1\theta_2} \end{pmatrix}$$

We define the following new aggregate variables for convenience:

$$\psi = \frac{\gamma}{\theta_1\theta_2}, \quad \phi = \eta\mu_1$$

Hence, the Jacobian becomes:

$$J = \begin{pmatrix} -\gamma & \theta_1 & 0 \\ 0 & -\psi & -\phi\psi^{-1} \\ \theta_2 & -\psi & -\phi\psi^{-1} \end{pmatrix}$$

Now we can find the form of the characteristic polynomial by taking the determinant of $(sI - J)$, where s is the solution to the polynomial, or the eigenvalues. For factorization purpose, it is convenient to do this with block matrices.

Suppose an arbitrary matrix M constructed from four block sub-matrices:

$$M = \begin{pmatrix} A & B \\ C & D \end{pmatrix}$$

$$\det(sI - M) = \det(sI - A)\det\left[(sI - D) - C(sI - A)^{-1}B\right]$$

We obtain the characteristic polynomial, or $\det(sI - J)$:

$$\begin{aligned} p(s) = \det(sI - J) &= (s+\gamma)\left[(s+\psi)\left(s + \frac{\phi}{\psi}\right) - \phi\right] + \frac{\phi}{\psi}\theta_1\theta_2\gamma \\ &= (s+\gamma)\left[s^2 + \left(\psi + \frac{\phi}{\psi}\right)s\right] + \frac{\phi}{\psi}\theta_1\theta_2\gamma \\ &= s(s+\gamma)\left[s + \left(\psi + \frac{\phi}{\psi}\right)\right] + \frac{\phi}{\psi}\theta_1\theta_2\gamma \end{aligned} \tag{4}$$

We note that, in the limit of strong binding and sequestration (large η, hence large ϕ), we can make the core assumptions that $\frac{\phi}{\psi} \gg \psi$ and also that root $s \ll \frac{\phi}{\psi}$ (Olsman, 2019). Setting $p(s) = 0$, we then have:

$$\begin{aligned} s(s+\gamma)\frac{\phi}{\psi} &= -\frac{\phi}{\psi}\theta_1\theta_2\gamma \\ s(s+\gamma) &= -\theta_1\theta_2\gamma \end{aligned} \tag{5}$$

In fact, from here, we can prove that the above antithetic circuit with one process node will be intrinsically stable, provided that the steady-state values are all positive. We will use the approach outlined in Olsman et al. (2019), in which we analyze the corresponding phase and magnitude constraints of the eigenvalues in the governing equation (5).

To ensure system stability, the eigenvalues must be either purely imaginary $\mathrm{Re}(s) = 0$, or complex with negative real part $\mathrm{Re}(s) < 0$. Geometrically, on the Argand plane, this corresponds to constraining the roots to the second quadrant, including the imaginary axis.

We now prove by contradiction by assuming that the opposite scenario where instability occurs (namely, when eigenvalues have positive real part). This happens when $s = a + bi$, with $a, b > 0$. Taking the complex argument both sides of (4):

$$\arg(s) + \arg(s + \gamma) = \pi \tag{6}$$

Because s has positive real part, it will always lie in the first quadrant of the Argand diagram. In other words:

$$0 < \arg(s) < \frac{\pi}{2}$$
$$0 < \arg(s + \gamma) < \frac{\pi}{2}$$

Hence:

$$0 < \arg(s) + \arg(s + \gamma) < \pi \tag{7}$$

This contradicts (6), and therefore there cannot be a solution to (5) with $\mathrm{Re}(s) > 0$. Therefore, the system must be stable.

We should emphasize that this favorable stability is simply because our antithetic circuit has solely one process node ($n = 1$). For more complex architectures with $n \geq 2$ $(x_1, x_2, ..., x_n)$, the stability criterion becomes more stringent and parameters must be tuned more rigidly. Detailed analysis of generalized n-node system is given in Olsman et al. (2019).

2.3 Model refinement

If we take into account the intrinsic removal of controller species (other than titration), the system of ODEs changes to:

$$\begin{cases} \dot{x} &= \theta_1 z_1 - \gamma_p x \\ \dot{z}_1 &= \mu_1 - \eta z_1 z_2 - \gamma_c z_1 \\ \dot{z}_2 &= \theta_2 x - \eta z_1 z_2 - \gamma_c z_2 \end{cases} \tag{8}$$

We can simplify this model further by assuming that the intrinsic removal for both the processor and controllers is only dictated by cytoplasmic dilution, or $\gamma_c = \gamma_p = \gamma$. Using similar methodology, it can be shown that this system is also intrinsically stable. As this model describes our experimental implementation

more accurately, we will therefore refer to it entirely in the following discussion and used it for further control theory analysis.

2.4 Global sensitivity analysis on simplified model

We then wish to explore the parameter space and how it affects the system's properties. To grasp the big picture, we performed a global sensitivity analysis (GSA) on the parameter set. This enabled us to quantify the extent to which slightly varying a certain parameter may cause a drastic change in the output. We relied on the SALib Python library, which contains various toolkit and methods for sensitivity analysis, enabling much more flexibility. The most common is the variance-based Sobol's method, which decomposes the variance of the model's output into fractions that can be attributed to the set of input parameters. The Sobol index is useful because it gives information not only on the first-order effect of a single parameter, but also on higher-order interactions between pairs. However, this method requires a specific sampling type called Saltelli sampling, which is computationally costly. Furthermore, for the test to be reliable, the sampling number must be at least 2^{15} (32768)! Still, it stands as a very powerful tool that we would return to in our complex network analysis (see later section).

Here, we decided to use the **Delta moment-independent measure**, which uses the delta (δ) index instead. We also used latin-hypercube sampling in place of Saltelli, which is known to reduce computer processing time by 50%, while still yielding relatively accurate results. The analysis was conducted with a sampling number of 10000. Figure 1 indicates the δ indices of each system's parameter on the steady state of species x, along with first-order Sobol's (S_1) for comparison. Note that we are interested only in the relative rank of the indices - the "importance" of the parameters, rather than the magnitude difference between the two methods. Bear in mind also that results from different methods may vary can to sampling errors.
We identified a satisfactory correlation of the two indices, showing that the processor's steady state is most sensitive to θ_2 and η. μ_1 and θ_1 follow behind, but with less agreement. We figured that the sequestration rate η depends entirely on the choice of titrator pairs, which posed more challenging to change. We therefore kept it constant, based on literature data of the sigma-antisigma pair; while freely varying θ_1, θ_2 and μ_1.

2.5 Parameter space

We then investigated parts of the parameter space and how it impacts the three steady states. It is noteworthy that, while we are mainly interested in the steady state of x, we also need to appreciate how the two controller species behave dynamically. It should be logical that, given the differences in magnitude and the difficulty of tuning the parameters into a perfect range, the concentrations of

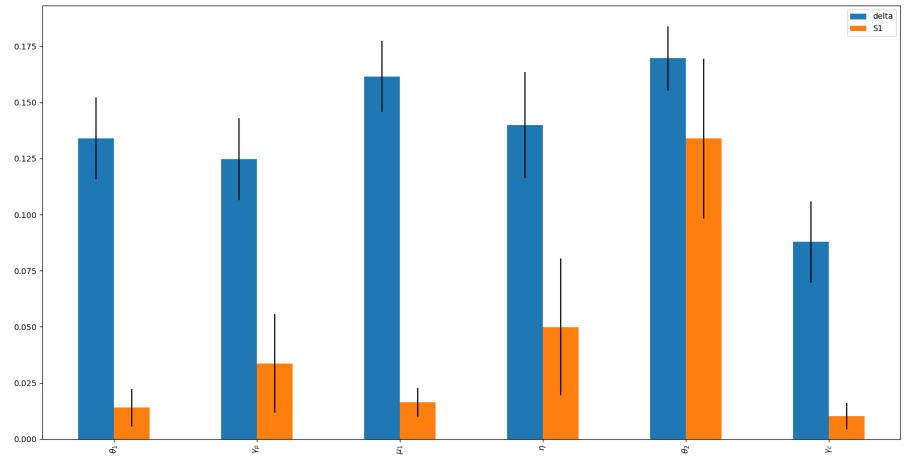

Figure 1: Global sensitivity analysis of the activation module using Delta moment-independent measure with latin-hypercube sampling, N = 10000. Given output for analysis is the steady state of process species x. S1 indicates first-order Sobol indices.

z_1 and z_2 at steady state will experience a high disparity. In other words, we would expect, in most cases, one species to reach a very high concentration, and the other to plummet. These scenarios are unfavorable, as high concentration will be toxic to the cells, while low concentration makes the circuit more prone to stochastic noise, reducing performance. It is therefore essential to look for parameter regions in which both steady states are appropriately calibrated.

Figure 2 illustrates a heatmap of steady states for the parameter pair $\theta_1 - \theta_2$. The color impression is scaled logarithmically to increase resolution. For the other constant parameters, we set $\gamma_p = \gamma_c = 3.8 \times 10^{-4}$ min^{-1}, $\eta = 5 \times 10^{-4}$ nM^{-1}min^{-1}, and $\mu_1 = 100$ nM min^{-1} Parameter ranges were rationally adapted from Aoki et al (2019), and the we arbitrarily chose the exact values within this range.

Figure 3 illustrates a heatmap of steady states for the parameter pair $\mu_1 - \theta_2$. θ_1 is kept constant at 1 min^{-1}, and the other parameters are set like described above. We did not consider $\mu_1 - \theta_1$ because, according to previous GSA, the output is not very sensitive to θ_1. Furthermore, it is practically more feasible to tune θ_2 using inducers (in this case, with OHC-14), than θ_1. We also note that as both parameters increase in magnitude, the system starts to behave erratically, as evident in the right corner of the plots. However, this range is only

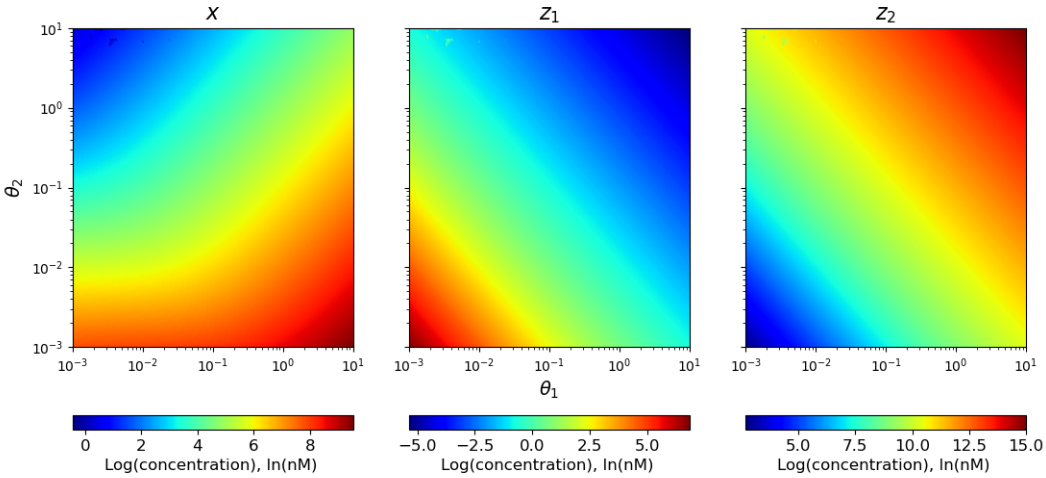

Figure 2: Heatmap surface of steady state of three species x, z_1 and z_2, in nM, with respect to θ_1 and θ_2 (min^{-1}) for activation module. $\gamma_p = \gamma_c = 3.8 \times 10^{-4}$ $\text{min}^{-1}, \eta = 5 \times 10^{-4}$ $\text{nM}^{-1}\text{min}^{-1}, \mu_1 = 100$ nM min^{-1}.

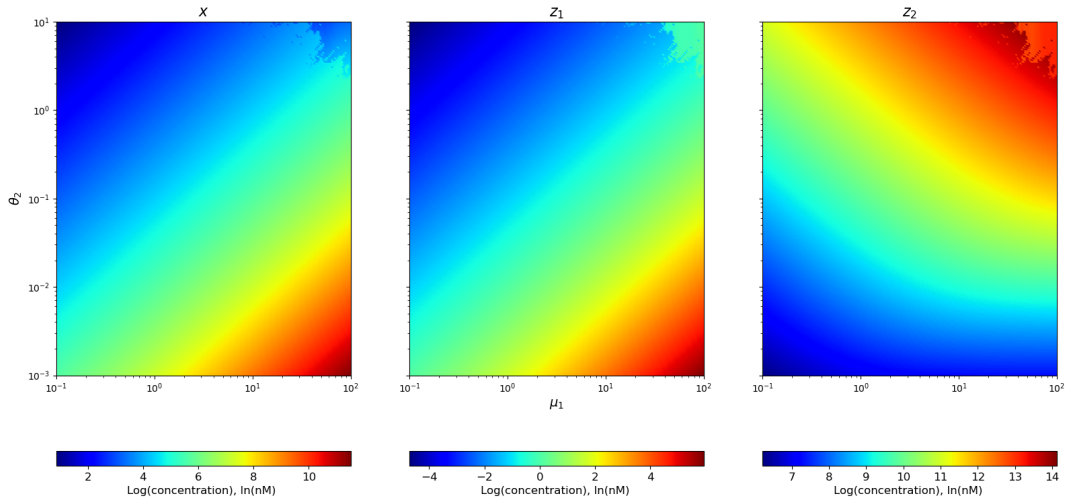

Figure 3: Heatmap surface of steady state of three species x, z_1 and z_2, in nM, with respect to μ_1 (nM min^{-1}) and θ_2 (min^{-1}) for activation module. $\gamma_p = \gamma_c = 3.8 \times 10^{-4}$ $\text{min}^{-1}, \eta = 5 \times 10^{-4}$ $\text{nM}^{-1}\text{min}^{-1}, \theta_1 = 1$ min^{-1}.

provisional for illustrative purpose, in practicality, both μ_1 and θ_2 are achieved at much lower values.

3 RPA in repression module

3.1 Model

We now turn our attention to the repression module. We first start by defining the following system of ODEs for the repression circuit **without intrinsic removal of controller species**:

$$\begin{cases} \dot{x} &= \dfrac{\alpha}{\theta_1 z_1 + 1} - \gamma x \\ \dot{z}_1 &= \mu_1 - \eta z_1 z_2 \\ \dot{z}_2 &= \dfrac{\mu_2}{\theta_2 x + 1} - \eta z_1 z_2 \end{cases} \tag{9}$$

Where α is the constitutive production rate of process species x, θ_1 is the repressive kinetic rate of controller z_1 acting on x, γ is the degradation (or dilution) rate, μ_1 and μ_2 are constitutive production rates of z_1 and z_2, respectively; η is the sequestration rate, and θ_2 is the repressive rate of x acting on z_2. Here, we spawn two new variables α and μ_2, which increases the dimension of parameter space.

This system is adapted from Olsman et al. (2019), but we only consider one process node ($n = 1$) instead of two, corresponding to our wet lab's implementation. Here, the repression dynamics is instead modelled in a non-linear fashion. In theory, we could have also done the same for activation module, but we want to showcase different analytic approaches along the way. Olsman et al. used a simplified Hill's function to represent the sigmoidal dynamics. The steady state values of each species are:

$$x_{eq} = \frac{\mu_2 - \mu_1}{\mu_1 \theta_2}, z_{1eq} = \frac{\alpha \mu_1 \theta_2 - \gamma\left(\mu_2 - \mu_1\right)}{\gamma \theta_1 \left(\mu_2 - \mu_1\right)}, z_{2eq} = \frac{\gamma \theta_1 \left(\mu_1 \mu_2 - \mu_1^2\right)}{\alpha \eta \mu_1 \theta_2 - \gamma \eta \left(\mu_2 - \mu_1\right)} \tag{10}$$

Before doing any analysis, we can see that for the steady-state of x to be biologically relevant and non-negative, μ_2 must be larger than μ_1.

3.2 Stability analysis

We linearize the system by taking the Jacobian (J):

$$\dot{\vec{x}} = J\vec{x}$$

$$J = \begin{pmatrix} -\gamma & -\frac{\alpha\theta_1}{(\theta_1 z_{1eq}+1)^2} & 0 \\ 0 & -z_{2eq}\eta & -z_{1eq}\eta \\ -\frac{\mu_2\theta_2}{(\theta_2 x_{eq}+1)^2} & -z_{2eq}\eta & -z_{1eq}\eta \end{pmatrix}$$

Plugging in the steady-state values, we obtain:

$$J = \begin{pmatrix} -\gamma & -\frac{\gamma^2(\mu_1-\mu_2)^2\theta_1}{\alpha\mu_1^2\theta_2^2} & 0 \\ 0 & \frac{\gamma(\mu_1-\mu_2)\mu_1\theta_1}{\alpha\mu_1\theta_2+\gamma\mu_1-\gamma\mu_2} & \frac{(\alpha\mu_1\theta_2+\gamma\mu_1-\gamma\mu_2)\eta}{\gamma(\mu_1-\mu_2)\theta_1} \\ -\frac{\mu_1^2\theta_2}{\mu_2} & \frac{\gamma(\mu_1-\mu_2)\mu_1\theta_1}{\alpha\mu_1\theta_2+\gamma\mu_1-\gamma\mu_2} & \frac{(\alpha\mu_1\theta_2+\gamma\mu_1-\gamma\mu_2)\eta}{\gamma(\mu_1-\mu_2)\theta_1} \end{pmatrix}$$

We define the following new aggregate variables for convenience:

$$\psi = \frac{\gamma\mu_1\theta_1(\mu_1-\mu_2)}{\alpha\mu_1\theta_2+\gamma\mu_1-\gamma\mu_2}, \quad \phi = \mu_1\eta$$

Hence, the Jacobian becomes:

$$J = \begin{pmatrix} -\gamma & -\frac{\gamma^2(\mu_1-\mu_2)^2\theta_1}{\alpha\mu_1^2\theta_2^2} & 0 \\ 0 & \psi & \phi/\psi \\ -\frac{\mu_1^2\theta_2}{\mu_2} & \psi & \phi/\psi \end{pmatrix}$$

We then obtain the characteristic polynomial, or $\det(sI-J)$:

$$\begin{aligned} p(s) = \det(sI-J) &= (s+\gamma)\left[(s+\psi)\left(s+\frac{\phi}{\psi}\right)-\phi\right]+\frac{\phi}{\psi}\frac{\theta_1\gamma^2(\mu_1-\mu_2)^2}{\alpha\mu_2\theta_2} \\ &= (s+\gamma)\left[s^2+\left(\psi+\frac{\phi}{\psi}\right)s\right]+\frac{\phi}{\psi}\frac{\theta_1\gamma^2(\mu_1-\mu_2)^2}{\alpha\mu_2\theta_2} \\ &= s(s+\gamma)\left[s+\left(\psi+\frac{\phi}{\psi}\right)\right]+\frac{\phi}{\psi}K \end{aligned} \tag{11}$$

Where we also define a new aggregate variable $K = \frac{\theta_1\gamma^2(\mu_1-\mu_2)^2}{\alpha\mu_2\theta_2}$. We note that, in the limit of strong binding and sequestration (large η, hence large ϕ), we make the core assumptions that $\frac{\phi}{\psi} \gg \psi$ and also that root $s \ll \frac{\phi}{\psi}$ (Olsman, 2019). Setting $p(s) = 0$, we then have:

$$\begin{aligned} s(s+\gamma)\frac{\phi}{\psi} &= -\frac{\phi}{\psi}K \\ s(s+\gamma) &= -K \end{aligned} \tag{12}$$

Using similar analysis, we can also show the system is intrinsically stable under **positive** steady-state values. This is important because for this case,

stability is only stringently possible for some positive sets of parameters. To find the parametric conditions for stability, we simply investigate the inequalities that govern the sign of the steady-state values. Referring back to (10), we work out the stability criteria:

$$\mu_2 > \mu_1 \tag{13}$$

$$\alpha\mu_1\theta_2 > \gamma\left(\mu_2 - \mu_1\right) \tag{14}$$

Inequality (13) can be achieved by tuning appropriate promoter strength. In other words, the gene encodes for z_2 should be under the control of a stronger promoter than that for z_1. Inequality (14), however, requires more careful analysis as five parameters are involved. But, as we are not changing the dilution rate γ, and assuming that we have firmly chosen μ_2 and μ_1, we just need to consider α and θ_2:

$$\alpha\theta_2 > \frac{\gamma\left(\mu_2 - \mu_1\right)}{\mu_1} \tag{15}$$

3.3 Model refinement

So far, we have omitted degradation of controller species z_1 and z_2 for tractable calculation. For the sake of completeness, let us now define a new system of ODEs where we take this into account:

$$\begin{cases} \dot{x} &= \dfrac{\alpha}{\theta_1 z_1 + 1} - \gamma x \\ \dot{z}_1 &= \mu_1 - \eta z_1 z_2 - \gamma z_1 \\ \dot{z}_2 &= \dfrac{\mu_2}{\theta_2 x + 1} - \eta z_1 z_2 - \gamma z_2 \end{cases} \tag{16}$$

Where γ is taken to be the same for all three species.

The non-linearity in (16) makes it unfeasible to derive an analytical expression for the equilibrium point. Yet, from preliminary parameter space screen, we observed that the system is surprisingly stable. We rationalized that the introduction of the terms $-\gamma z_1$ and $-\gamma z_2$ causes the system to behave like a **leaky integrator**, which actually reinforces stability. This makes sense, as instability arises due to the production rate overwhelming the removal rate. By having additional removal terms (or increasing the leak), the system can combat its high production rate. More in-depth explanation is given in the control theory section.

3.4 Global Sensitivity Analysis on simplified model

We now conduct GSA on the repression module using the previously described Delta moment-independent measure (Figure 4). The Sobol and δ indices do not correlate well for α, but consistently show that θ_1 is the most significant on every reruns (not shown), followed by either α or μ_1.

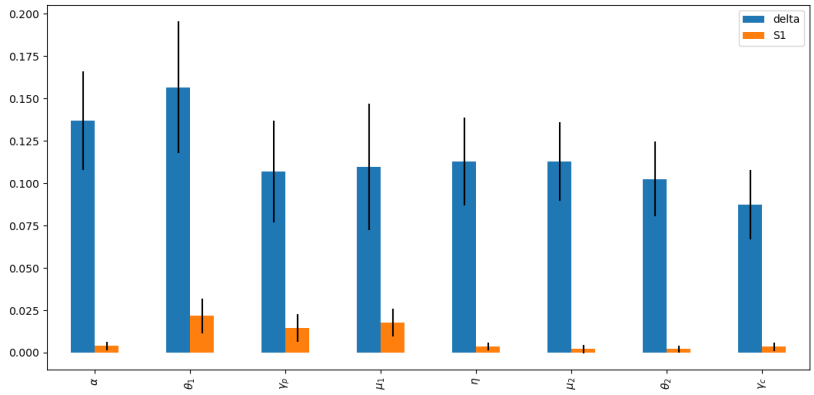

Figure 4: Global sensitivity analysis of the repression module using Delta moment-independent measure with latin-hypercube sampling, N = 10000. Given output for analysis is the steady state of process species x. S1 indicates first-order Sobol's indices.

3.5 Parameter space

We investigate the pair μ_1 - μ_2, as they are the most feasible to implement (Figure 5). Similar to the case for activation module, we set the other parameters arbitrarily constant within the acceptable range of magnitudes. We also take this opportunity to demonstrate that if there is no removal of z_1 and z_2 ($\gamma_p = 0$), the stability region is significantly more constrained (Figure 6)

3.6 Positive perturbation

For the final piece of analysis, we wish to quantify the effect of positive perturbation on the system's performance, in line with our wet-lab implementation (see circuit design page). We shall omit the controllers' removal term once again for simpler manipulation, but add a perturbation term:

$$\begin{cases} \dot{x} &= \dfrac{\alpha}{\theta_1 z_1 + 1} - \gamma x + \beta \\ \dot{z}_1 &= \mu_1 - \eta z_1 z_2 \\ \dot{z}_2 &= \dfrac{\mu_2}{\theta_2 x + 1} - \eta z_1 z_2 \end{cases} \tag{17}$$

Where β is a constant parameter for perturbation. We obtain a new equilibrium state expression:

$$x_{eq} = \frac{\mu_2 - \mu_1}{\mu_1 \theta_2}, z_{1eq} = \frac{(\alpha+\beta)\,\mu_1\theta_2 - \gamma\,(\mu_2 - \mu_1)}{\gamma\theta_1\,(\mu_2 - \mu_1) - \beta\mu_1\theta_1\theta_2}, z_{2eq} = \frac{\beta\mu_1^2\theta_1\theta_2 - \gamma\theta_1\left(\mu_1\mu_2 - \mu_1^2\right)}{(\alpha+\beta)\eta\mu_1\theta_2 - \gamma\eta\,(\mu_2 - \mu_1)} \tag{18}$$

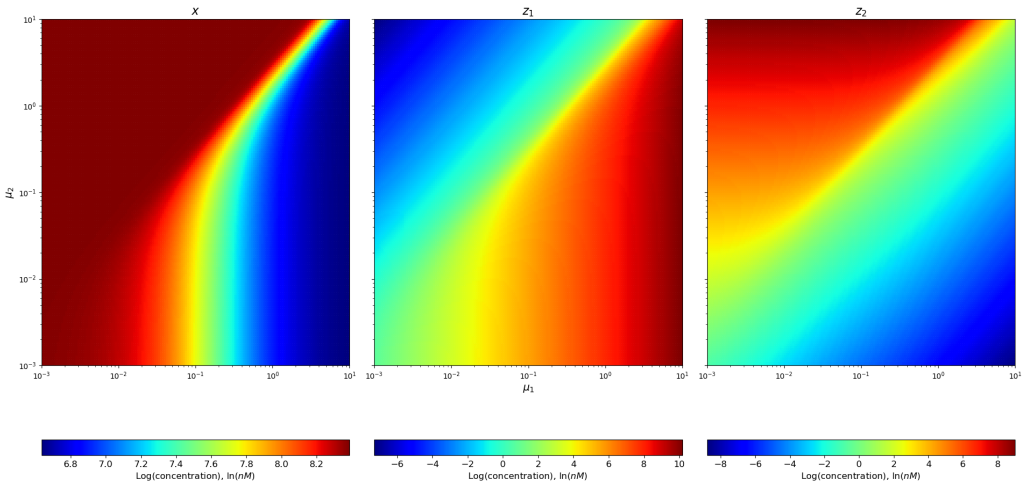

Figure 5: Heatmap surface of steady states of three species x, z_1 and z_2, in nM, with respect to μ_1 and μ_2 (nM min^{-1}) for repression module. $\alpha = 10$ nM min^{-1} , $\gamma_p = \gamma_c = 3.8 \times 10^{-4}$ min^{-1}, $\eta = 5 \times 10^{-4}$ $\text{nM}^{-1}\text{min}^{-1}$, $\theta_1 = 10^{-2}$ min^{-1}, and $\theta_2 = 10^{-3}$ min^{-1}.

This is more complicated, but still manageable. To impose stability, the equilibrium point must be all positive (explained above). Performing simple algebraic manipulation, we yield the bounded inequalities:

$$\boxed{\mu_2 > \mu_1} \tag{19}$$

$$\boxed{\frac{\gamma}{(\alpha+\beta)\,\theta_2+\gamma} < \frac{\mu_1}{\mu_2} < \frac{\gamma}{\beta\theta_2+\gamma}} \tag{20}$$

The inequality is useful since we can collect the parameters μ_1 and μ_2 into a single aggregate ratio. If we assume that $(\alpha+\beta)\,\theta_2,\ \beta\theta_2 \gg \gamma$ (usually, dilution rate is much slower than the rest), we can further simplify (20):

$$\frac{\gamma}{\alpha+\beta} \ < \ \frac{\mu_1}{\mu_2}\theta_2 \ < \ \frac{\gamma}{\beta} \tag{21}$$

This criterion is biologically relevant. We observe that:

- Increasing the perturbation, and hence the stress to the system, (β in the denominator) will narrow both lower and upper bounds, making it more stringent to tune the parameters within stable range.
- In contrast, higher γ will broaden the bounds, corroborating with the behavior of a leaky integrator (see above).

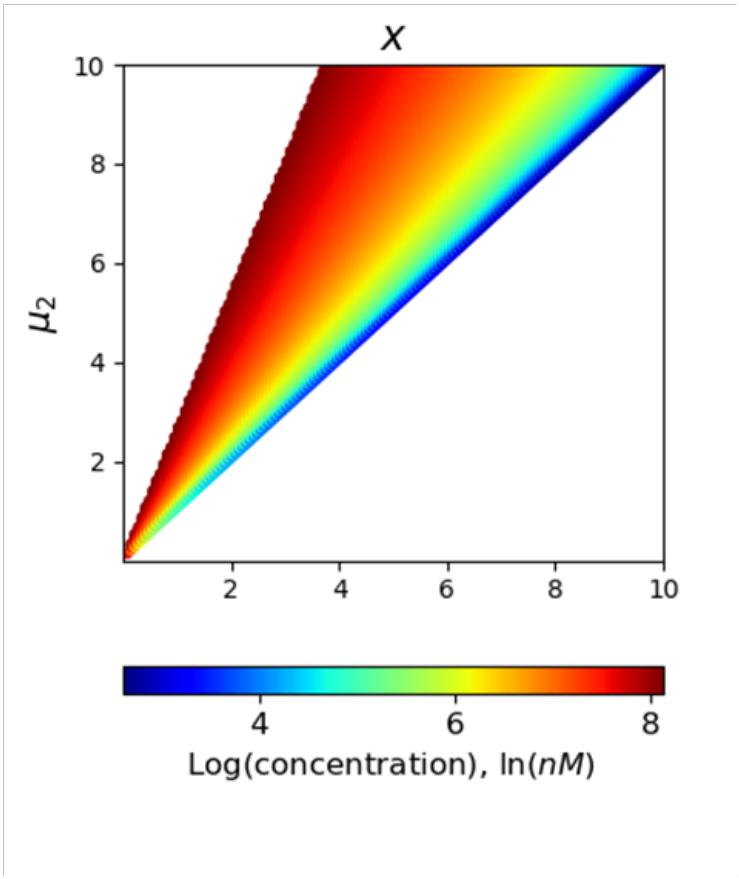

Figure 6: Heatmap surface of steady states of three species x, z_1 and z_2, in nM, with respect to μ_1 and μ_2 (nM min^{-1}) for the repression module **without controllers degradation**. White region indicates instability, and the axes are shrunken down to linear scale. $\alpha = 10$ nM min^{-1} $\gamma_p = 3.8 \times 10^{-4}$ $\text{min}^{-1}, \gamma_c = 0$ $\text{min}^{-1}, \eta = 5 \times 10^{-4}$ $\text{nM}^{-1}\text{min}^{-1}$, $\theta_1 = 10^{-2}$ min^{-1}, and $\theta_2 = 10^{-3}$ min^{-1}.

- Increasing α - the maximal production rate of x, will push back the lower bound, thus also widening the range.

Looking carefully, we see that the steady state of x is independent of β and is equivalent to the case without perturbation ($x_{eq} = \frac{\mu_2 - \mu_1}{\mu_1 \theta_2}$). We briefly showed that, mathematically, even under perturbation, the steady state of process species must remain unchanged. This is true only if the system is stable. In other words, for the case without considering intrinsic removal of z_1 and z_2, **stability is coupled with RPA**, and as long as the bounds in is achieved, we should expect the system to be both stable and perfectly adapt.

Of course, when taking into account the removal rate γ_c, we are no longer able to obtain the analytic expressions for steady states, and thus the inequality no longer holds. Still, using this criterion we get a rough estimation of the neighborhood in the parameter space. We can, however, look at the offset (or steady-state error), between perturbed and unperturbed systems and determine what range of parameters would give the lowest offset. For this example (Figure 7, we chose an arbitrary value of 0.1 nM min^{-1} for β, which can be flexibly tune using an inducible perturbation circuit (see Design page). Here, we define the **relative offset** as:

$$\text{Relative offset} = \frac{|s_{eq}(\beta = 0) - s_{eq}(\beta \neq 0)|}{s_{eq}(\beta = 0)}$$

We can see that the region for near-perfect adaptation is more stringent for this particular set of parameters.

Further perturbation analysis will be discussed in the control theory section.

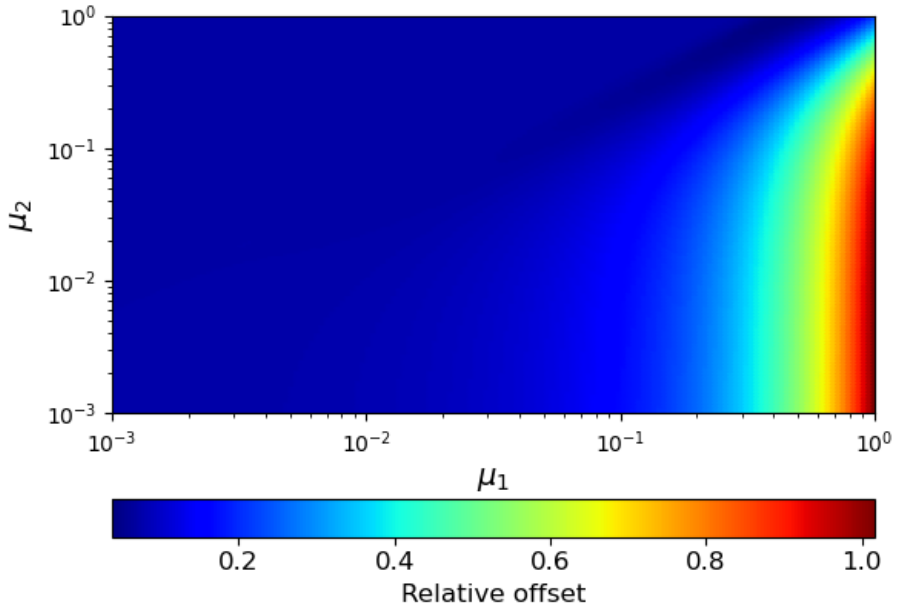

Figure 7: Heatmap surface of relative offset of x, with respect to μ_1 and μ_2 (nM min^{-1}) for repression module. $\alpha = 10$ nM min^{-1} , $\gamma_p = \gamma_c = 3.8 \times 10^{-4}$ min^{-1}, $\eta = 5 \times 10^{-4}$ $\text{nM}^{-1}\text{min}^{-1}$, $\theta_1 = 10^{-2}$ min^{-1}, and $\theta_2 = 10^{-3}$ min^{-1}. $\beta = 0.1$ nM min^{-1}. Axes are rescaled to offset < 1.